

# Application of Remote Sensing in the Identification and Extraction of Lineaments and the Calculation of Mining Showings in the Mesozoic Cover of the TAZEKKA Massif of Morocco (Maghraoua Region)

J. CHOUKRAD<sup>1,2</sup>, A. ELMOUSSALIM<sup>2</sup>, N. SAOUD<sup>1,2</sup>, S. MOUNIR<sup>1</sup>, N. ASSABAR<sup>1</sup>, A. AITALI<sup>1</sup>, M. CHARROUD<sup>1</sup>

<sup>1</sup>Laboratory of Intelligent Systems, Georesources & Renewable Energies (SIGER) FST-USMBA, Fes, Morocco

<sup>2</sup>Department of Research & Development - ATLAS MINING

**Abstract**— This work describes the procedure followed in mineral exploration based on the production of index maps via the use and processing of satellite images, the use of remote sensing and geological research in order to make a detailed mapping of the different mineralization indices of the Mesozoic cover of Tazekka (Maghraoua region).

**Keywords**— Remote Sensing, Satellite Images, Mineralization and Liassic Cover of Tazekka

## I. INTRODUCTION

Remote sensing exhibits a set of tools to perfect the localization of geological structures and mining indices, from processed satellite image which constitutes a vigorous source of information when it is assembled with the data collected following geological investigations of ground.

This work consists to the mapping and the interpretation of the geological structures of Liassic cover of Tazekka Hercynian massif, which is extracted automatically by satellite image processing methods, being a methodological approach in the identification of areas with mining potential. The choice of the zone study is based on the presence of numerous indications of mineralization and several mines as Ain Aouda, Boujaada and Dar Bou Azza..... In fact the almost goal is the identification and the monitoring of mining showing occurred in the zone study using remote sensing methods.

## II. PRESENTATION OF ZONE STUDY

The zone study is located at the NE of the Hercynian massif of Tazekka, located in its turn in the north-eastern part of the chain of the Middle Atlas of Morocco (Fig. 1), and more

precisely about twenty kilometers to the SW of the city of Taza, it is covered by the topographic map of Taza and Msoun at 1/50 000).



Fig. 1: Geographical map of the Tazekka massif

In the Hercynian massif of Tazekka, the Paleozoic corresponds successively to (Fig. 2): Cambro-Ordovician formations, consisting of purplish schist (wine lees) or gray-green, comprising schist argillites with thin micaceous sandstone beds, gresopelites mainly pelites and silts, and grauwackeux sandstones. These deposits are interpreted as a strato and grano-increasing mega-sequence of subsident platform type. These schisteous formations are discordantly surmounted by Triassic facies comprising two series of red argillites separated by a doleritic basaltic complex. The meso-Cenozoic sedimentary series encountered in the sector have an age that ranges from the Triassic to the Lower Aleno-Bajoc in the Tazekka region (AUJJAR J. (2000)), The triassic consists of two series of red argillites separated by a volcanic

complex. The Liassic deposits formed successively of brecciform, fine and gray dolomites with Birdeyes type structures of Lotharingian age, various limestones with facies of shallow platform which marks the beginning of the Carixian and oolitic limestones in large banks of Domesian age (Fig. 2).

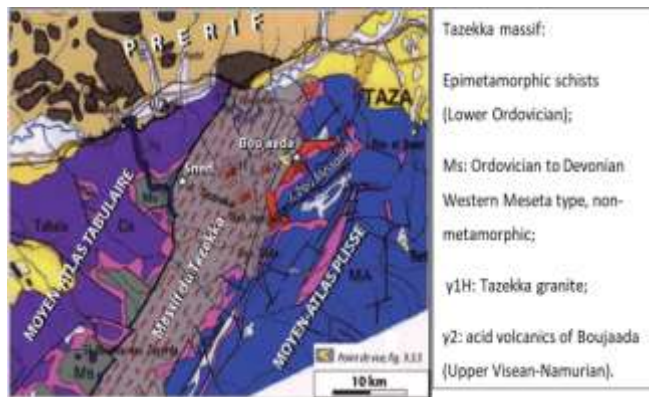


Fig. 2: Simplified map of the Tazekka massif (extract from the structural map of the Rif in à 1/500 000

### A. Mineralization's

In the Paleozoic basement of the Tazekka, veins of BPGC type veins appear quartz-barytic stockworks and Sb, As-Fe, Sn, W and Mo mineralization's. These mineralizations are hosted in the three formations of the Palaeozoic base, namely shales of the Lower Ordovician, the volcano-sedimentary series of the Upper Visean-Namurian and the Tazekka granite.

At the level of its Mesozoic cover, corresponding to a Liassic carbonate platform, mineralization's essentially lead-zinciferous and ferrified appear. These latter appear on the ground in the form of a horizontal zone at Pb-Zn showing the paleogeographic and structural characteristics controlling the geographical distribution of these mineralization's.

## III. MATERIALS AND METHODS

The main objective of this work includes a new approach to mineral exploration, which consists in using remote sensing as a method of distal geological investigation, namely how to detect mineral showings; to confirm the presence of these clues. The presentation of the remit of remote sensing to mineral prospecting during the first exploration phases helped to avoid the obstacles encountered in terms of raising the cost of exploration and the time necessary for the completion of the stages of geological prospecting. During this work, the various data collected will be confirmed by field studies and correlated with geochemical data.

In the study area at the study area level, this is characterized by the presence of a variety of Pb-Zn, Fe mineralization generated by the succession of geological and geodynamic events. In fact, this study consists in highlighting the geographic distribution of numerous mineralizations' that are not yet identified. To do so, we focused our work on the structural and mineralogical cartography of the study area based on remote sensing approaches (Karimpour et al., 2008).

### A. Preprocessing of the satellite image

The preprocessing operations consisted of radiometric and geometric corrections. The geometric correction carried out according to the polynomial method makes it possible to correct the various distortions caused by the environment (curvature of the earth, variation in altitude of the ground, etc.), originating from the movement of the platform, and due to the errors of the measurement systems. Radiometric correction corrects image errors generally caused by atmospheric disturbances (Markham et al., 2015).

### B. Contrast enhancement or enhancement

The corrected images were processed in order to increase the visual perception of the image, improving its quality and making it more expressive. These various tasks are accomplished with a view to better visualization or observation of discontinuities. Among the many image enhancement techniques, the following techniques have been applied: the Hotelling transform (ACP), image combinations, color compositions and spatial filtering. (Song et al., 2001)

**1) Landsat sensors:** RBV sensors: On the first two satellites, the series of 3 video cameras was taking visible and infrared images. The resolution was 80 m for images of 185 km by 185 km. On LANDSAT 3, the resolution was increased to 40 m, but the cameras only took pictures in a single panchromatic spectral band (0.5 - 0.75  $\mu\text{m}$ ) (Forster, B. C. (1984)).

MSS sensors: These mechanical scanners recorded information in four spectral bands and over an area of 185 km by 185 km. As these instruments were developed after the three RBV cameras, these bands were numbered from 4 to 7 (Zuckerman, B et al, 2001) The MSS sensor of LANDSAT 3 included an additional spectral band in thermal infrared.

TM sensors: These high resolution scanners have 7 spectral bands and always cover an area of 185 km by 185 km.

ETM + sensor: This scanner is an evolution of previous TMs. It now has a wide panchromatic band at high resolution.

Thermal infrared sensor (TIRS): The thermal infrared sensor (TIRS) will measure the earth's surface temperature in two thermal bands with a new technology that applies quantum physics to detect heat (Corral et al., 2011).

OLI sensor: will measure in the visible, near infrared and short infrared waves of the spectrum. Its images will have 15 meters panchromatic and 30 meters of spatial multi-spectral resolution along a 185 km. (BONN.F et al, 1992).

## IV. RESULTS

### A. Image processing

**1) Linear array extraction:** Manual extraction of lineaments is used in this study. Indeed, the lineaments are the linear structures observed on the satellite images except the

anthropological linearities (track, roads, and high voltage wires).

The validation of the map of lineaments consists of accomplishing the following tasks:

- Comparison of directional rosettes;
- Use of field data.
- Use of Google Earth images
- Comparison of the results obtained with that of the geological literature of the region.

Manual extraction consists in digitizing any linear structure observed on the image while ignoring anthropic linearity's (tracks, roads, high-voltage wires) by superimposing vector layers on images (Bodin et Razack, 1999). Fracture is obtained after validation of the lineament network (Fig. 3).

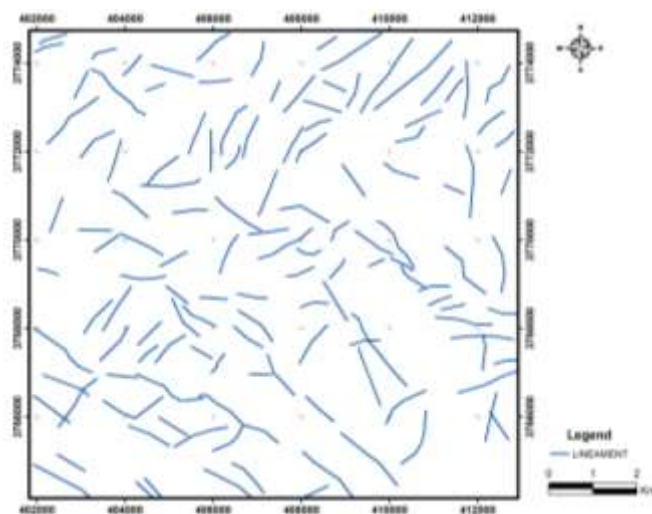


Fig. 3: Result of the main component analysis of the lineaments extracted by the main component of ACP band 1

**2) Validation of the lineament network:** Filtering in the four main directions (N0, N45, N90 and N135) (Fig. 4) of the first main component and of band 5 made it possible to draw a map of lineaments. The combination of the two lineament maps from band 5 and the ACP1 makes it possible to establish a synthetic map of the lineaments of the Si study area (Mhamedi et al., 2016). The correction of this map of lineaments consists in eliminating the linear structures (Road, River, Crest line...), correcting the geometry and eliminating the redundancies of lineament (Alaa, 2006). The validation of the result is done first by Google Earth images (Fig. 5), and secondly by pre-existing data and field missions.

Facies mapping by combined approach of the terrain and remote sensing

The combination of false color images, band ratios and the main component band (PC) (Decaestecker and Saerens, 2008) has given good results in discriminating different sedimentary facies. By comparing the results obtained with the 1/50000 geological map of Taza, we observe that the presence of the superposition of certain limits of the geological formations. The colored combination of the ratio bands (3-6-6 / 7) (Kouamé et al., 1999) also allows better separation of Liassic facies and Triassic Clays (Fig. 6).

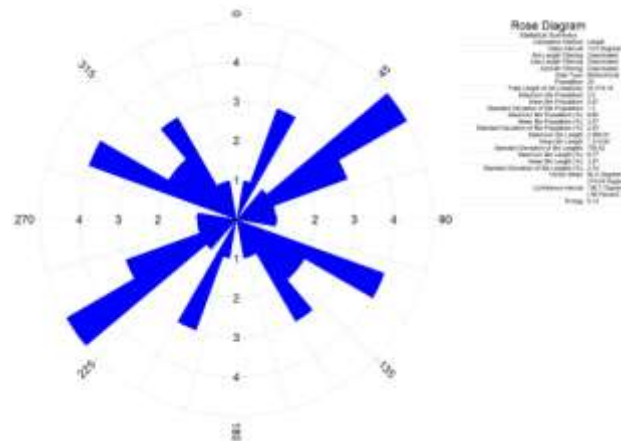


Fig. 4: Rosette of the different lineaments of the region of Tazekka and their frequency



Fig. 5: Example of validation of lineament, with a Google Earth image

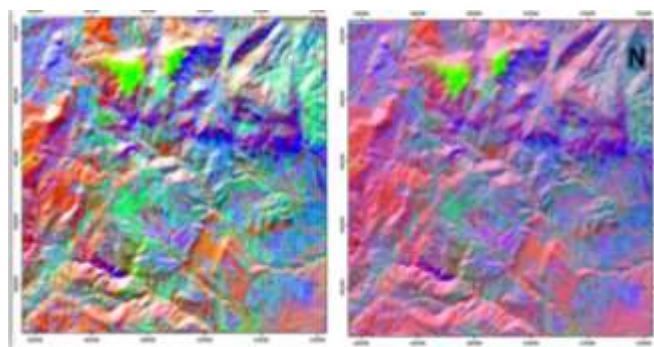


Fig. 6: Map of the Tazekka region using analysis with the main component

**3) Control validation and Interpretation of results:** The superimposition of the geological map with the processing of satellite images makes it possible to draw the limits of the geological formations; subsequently these data were confirmed in the field (Fig. 7).

The combination of remote sensing results and field missions enabled us to produce a geological map of the border and the Tazekka Massif (Fig. 2). The Taza map shows the

presence of formations stretching from the Triassic to the Upper Liass. Particular interest was given to the detailed cartography of the Jurassic, because it is the objective of our work.

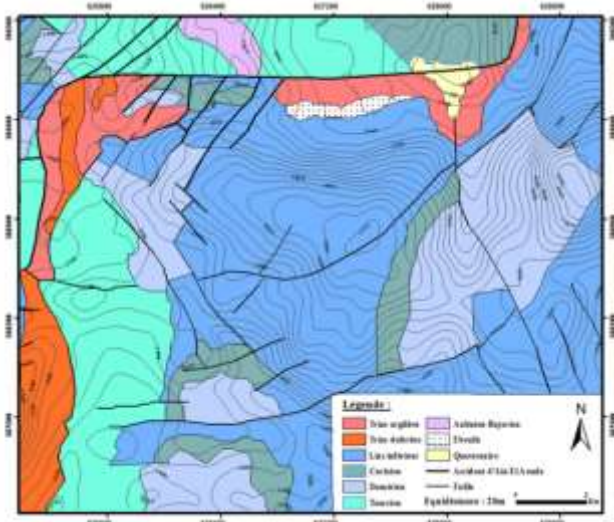


Fig. 7: Geological mapping using analysis with the main component

**B. Processing and calculation of indices**

The use of Landsat TM satellite images for the calculation of weathering mineral indices From the Middle Atlas of Tazekka (Maghraoua region) is a step that can intervene in the research and study phase for mineral exploration.

**1) Simple vegetation index:** It is an indicator given by the software from the image "TAZA" (Fig. 8), the calculation is done by the following formula: band 4 - band 3 (BONN.F and all 1992):

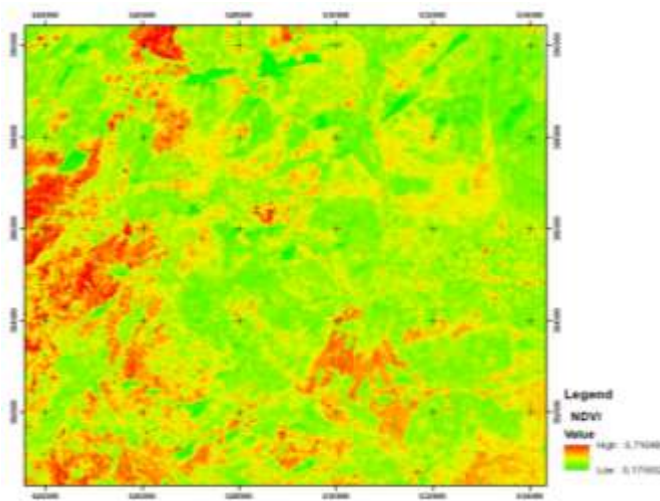


Fig. 8: Simple vegetation index map extracted from the Landsat image of the eastern part of Tazekka

The plant cover in the "Tazekka" massif occupies a large area at the level of the Middle Atlas due to the presence of

water and favorable conditions. In the study area, we note that the vegetation is abundant in the eastern part and the southern part.

**2) Ferrous Minerals Index:** The ferrous minerals index (Fig. 9) is obtained following the application of the TM5 / TM4 ratio (Segal, D 1982; Drury, S. 1987).

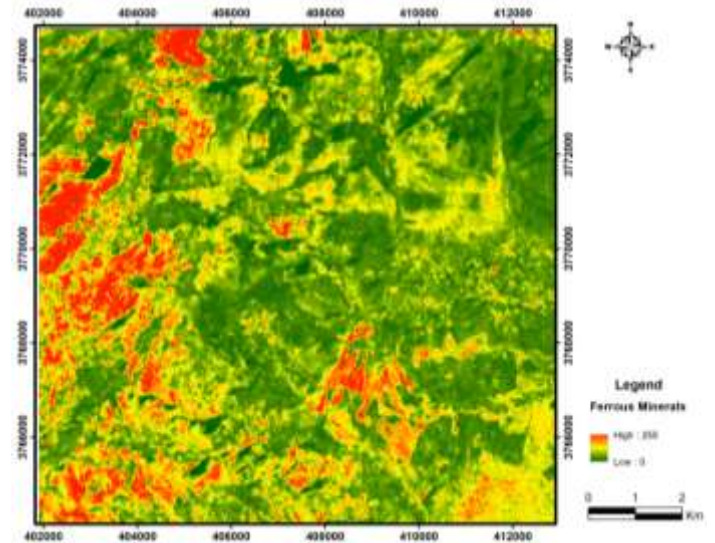


Fig. 9: Ferrous Minerals Index

The treatment of the ferrous minerals index shows zones with significant potential, located to the West, the NW and the SSE part. These indices were confirmed by the geological map and geochemical analyzes showing a correlation between the two.



Fig. 10: index of ferrous minerals in the anomaly zone

The example of the Ain aouda mine located in the NW, this region proves overwhelmingly this high potential of ferrous minerals.

On this deposit, the mineralization consists essentially of iron oxides and zinc oxides and sulfurous minerals.

The treatment of the ferrous minerals index shows 3 important zones, SE, NW and part W, with a comparison with the iron indices on the geological map shows a correlation between the two. The example of the Ain Aouda mine (Fig. 16), where structures from the Middle Atlas come to join it (Robillard, D. 1981). south of the great E-W fault this region is essential proof of the confirmation of this high potential of ferrous minerals. On this deposit, the primary mineralization in the form of sulphides is represented by chalcocite, chalcopyrite, pyrite, bornite, covellite, and rarely proustite. Secondary minerals are also present. These are iron oxides and hydroxides (hematite, goethite, and limonite), copper oxide (cuprite) and copper carbonate and hydrocarbon (malachite, azurite).

3) **Clay minerals:** The clay mineral index (Fig. 11), it is obtained by the function band5 / band7.

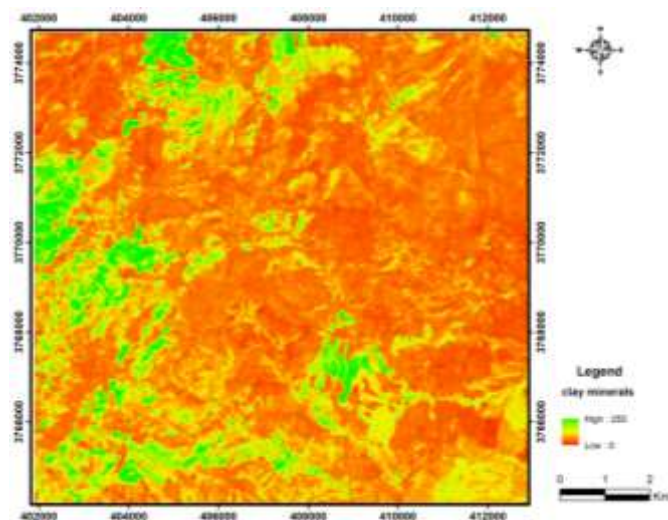


Fig. 11: clay mineral index

Analysis of the Figure shows that the clay minerals (Fig. 12) are localized with a high concentration of W, S and the N part, thanks to the presence of dense vegetation which helps in the formation of soils by the physical disintegration of the rock by the penetration of the roots, and the decomposition of organic matter.

The superimposition of the geological map with the processing of satellite images makes it possible to draw the limits of the geological formations; subsequently these data were confirmed in the field, which helped us to produce a geological map for the study area (Fig. 7).

The argillaceous formation of the Triassic is located to the west of the study area, it extends to the NW along the fault in the EW direction, namely that the zones with mineral potential settle in the Triassic. The dominant formation in this area is the limestone of the Liass as well as the carbonates of the Domerian and the Toarcian.

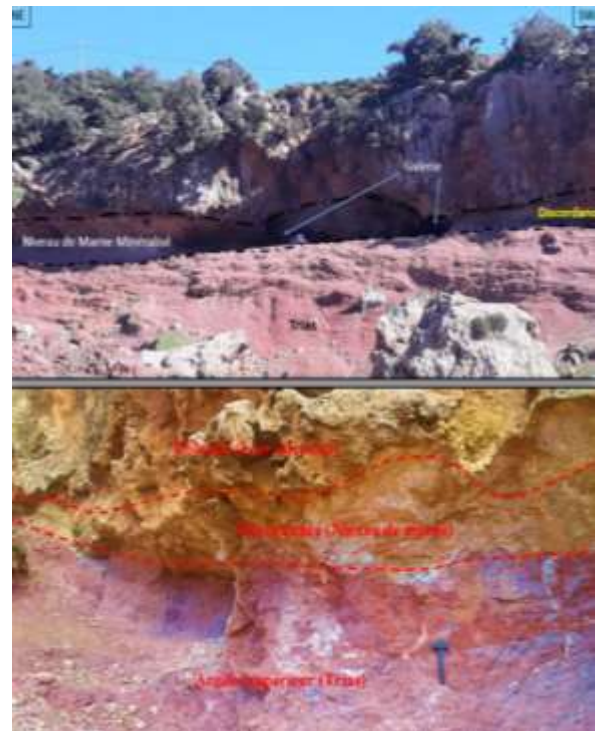


Fig. 12: contact zone Upper clay - Lower dome with evidence of clay mineralization

**Iron oxide:** The iron oxide index (Fig. 13), it is represented by the function band3 / band1 (Hewson, Rob D. 2001).

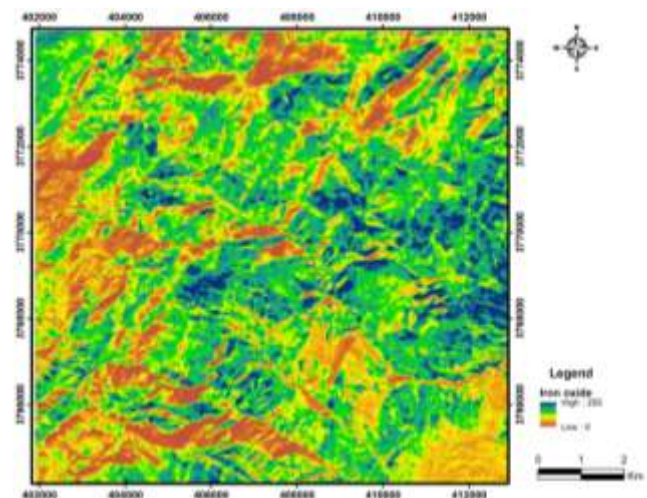


Fig. 13: Iron oxide index

The iron oxide index is shown on the map with high concentrations, mainly in the northern and southern parts. Namely, those iron oxides are distributed randomly in the ground mainly in the North West part of Ain Aouda and in the polymetallic deposit of Maghraoua.

The Ain El Aouda deposit and the Maghraoua polymetallic deposit produced approximately 4000 tonnes of calamine at 48% Zn, or approximately 2000 tonnes of metal (unpublished

document) (AUJJAR J. 2000). It is the most important zinciferous mass in the folded Middle Atlas domain.



Fig. 14: Iron oxide index in the dolomitic breccias of the Tazekka Liassic cover.

**4) Hydrothermal composite:** The hydrothermal index calculation (Fig. 15) is done by 3 band5 / band4 applications, 4/3 and 5/7 (Sabins, 1999).

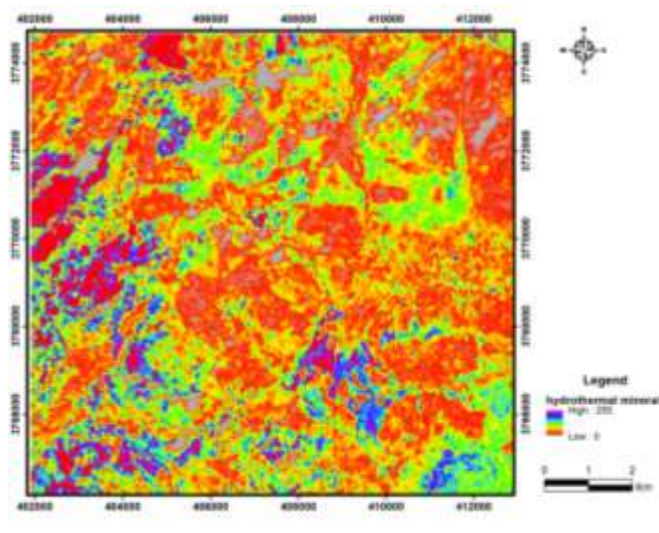


Fig. 15: Hydrothermal composite

The analysis of the hydrothermal mineral index map shows a significant concentration in the North, West and South part, this mineralization is confirmed by indices extracted from the geological map which are located in hydrothermal mineral deposits (Fe, Zn, Pb).

From the analysis of the hydrothermal minerals index card, we note that the northern part and the central part have a high concentration compared to the other zones.

The indications detected by the landsat satellite are confirmed by indices extracted from the geological map. They are located in hydrothermal mineral deposits (Cu, Zn, Pb).

Among these, the Polymetallic deposits of Ain Aouda boujaada, and ain aouda, where the mineralization is formed by Pb and Zn.

The distribution of indices on the global map shows areas of coincidence between them. Regarding ferrous indices, iron oxides and hydrothermal indices, we can conclude that these are the same processes that gave these anomalies. Others parts the relationship between the clay minerals index and the vegetation are explained by the importance of one before the other.

Field observations show that the Ain Aouda scale mass falls within the limits of a quarry (Fig. 16) characterized by plurimetric cavities or pockets filled with red clays, limonites and hematite (Fig. 10).

On the wall of the quarry, the development of a gray dolomite around a small karstic cavity with oxidized Zn is clearly visible (Fig. 16).

The mineralization also contains blende and galena associated with cerusite. We also find smithsonite, hemimorphite, barite and calcite geodes as well as iron oxides which come in cubes attesting to its primitive sulfur nature.

We would therefore have mineralization of blende, pyrite and galena origin. The dissemination of pyrite would have facilitated the oxidation of the blende. This sulfurized mineralization has been affected by recent karstification, the result of which is the formation of Zn oxides.

The lower Lias, characterized by dolomitic carbonate formations which characterize the deposition environments by their textures and structures, in the ground is:

- A fractured dark gray dolomite contains veinlets of sulphides (A).
- A light gray dolomite with calcite veins (B).
- A gray dolomite with hydrothermal activity of Fe and Zn oxide, we also find traces of quartz and limonite.



Fig. 16: indices and field data on the presence of mineralization in the study area

## V. DISCUSSION

The framing map of the Tazekka region (Middle Atlas) was made possible thanks to the application on Landsat TM satellite images, the techniques of analysis of satellite images allowing the highlighting of networks of major lineaments. The map obtained after the satellite image processing by the directional filters (spatial enhancement), The results obtained by the visual and statistical analysis of the map of lineaments, shows that these lineaments are divided into two main families of direction; The first family and direction N120; The second family and direction N35 to N45.

The comparison of the tele-analytical linear map extracted from a satellite image and the geological map shows similar directions. However in terms of staff, there is an abundance of lineaments extracted from the satellite image compared to those from the geological map.

The processing of the satellite image of the region of Tazekka used to establish mineralization index maps is an essential tool in remote sensing in the field of mineral prospecting. Analysis of these maps shows a number of important geological information:

The iron oxide index is intimately linked to the red Triassic formations, located in the eastern part of the Tazekka Inlier.

Ferrous minerals occur with significant concentrations in the NW, SE and E parts of the eastern sector of Tazekka. We note that these minerals have a high concentration north of mghraoua and which coincides with an already exploited mining zone, the mine of ain aouda. The hydrothermal minerals map shows high concentrations in the central part of the study area, particularly in the area of the Maghraoua deposit. This last coincidence constitutes a validation of the hydrothermal minerals map as a prospecting guide. The clay minerals map shows a high concentration in the western part of the sector, on which the vegetation occupies a large area this is explained by the richness of the clay soils.

The superposition of the mineral showing maps and the fracturing map shows that the potential zones of mineralization are affected by generally NW-SE direction faults (Fig.17).

In the end, the superposition of the index maps and that of the lineaments extracted from the satellite image, with the geological map of the study area allowed us to obtain a final map which is considered as a starting point to complete the prospecting mining in the field, and guide all geological investigation work.

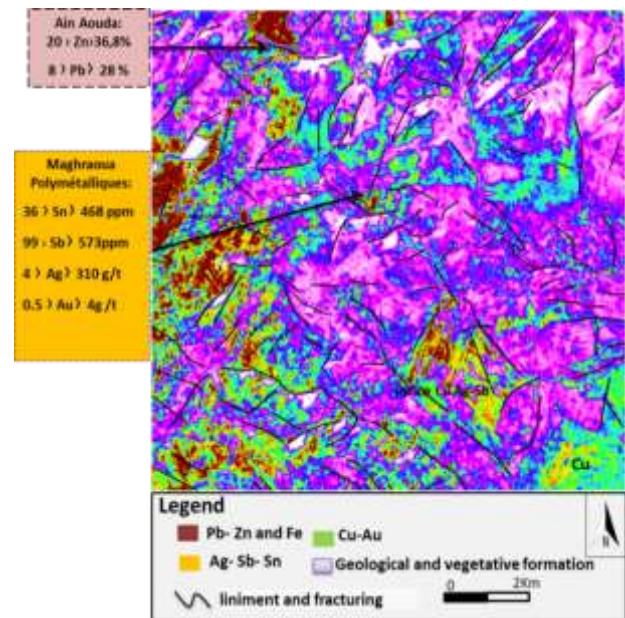


Fig. 17: Map of the distribution of mining showings

## REFERENCES

- AA, M. & KOIKE, K., 2006, Tectonic architecture through Landsat-7 ETM+/SRTM DEM-derived lineaments and relationship to the hydrogeologic setting in Siwa region, NW Egypt. *Journal of African Earth Sciences*, 45, pp. 467–477.
- AUAJJAR J. (2000) : Aperçu structural de la boutonnière du Tazekka (socle et couverture). MEMOIRE DU SERVICE GEOLOGIQUE N°390, p.31-32-33-17-53-54.
- Bodin J. & Razack M. (1999) L'analyse d'images appliquée au traitement automatique de champs de fractures. Propriétés géométriques et lois d'échelle. *Bulletin de la Société Géologique de France*, t. 170, n°. 4, p. 579-593.
- ONN.F et all 1992: 'A review of vegetation indices', *Remote Sensing Reviews*, 13: 1, 95-120.
- ORRAL, I., GONZÁLEZ, F., GRIERA, A., CORBELLA, M., GÓMEZ-GRAS, D. & CARDELLACH, E., 2011, Landsat ETM+ Imaging for the Exploration of Epithermal Deposits in the Azuero Peninsula (Panama). *macla*, 15, pp. 67-68.
- Decaestecker et Saerens, 2008: Link-based community detection with the sigmoid commute-time kernel: A comparative study.
- Drury, S. *Image Interpretation in Geology*. London: Allen and Unwin (1987), 243 pp.
- Forster, B. C. (1984): Derivation of atmospheric correction procedures for Landsat MSS with particular reference to urban data. *Int. J. Remote Sens.* 5:799–817
- Hewson, Rob D.; Cudahy, T. J.; Huntington, J. F. (2001): *Geologic and alteration mapping at Mt Fitton, South Australia, using ASTER satellite-borne data* Vol. 2, p. 724-726
- KARIMPOUR, M.H., MALEKZADEH SHAFAROUFI, A., STERN, C.R. & HIDARIAN, M.R., 2008, Using ETM+ and Airborne Geophysics Data to Locating Porphyry Copper and Epithermal Gold Deposits in Eastern Iran. *Journal of Applied Sciences*, 8, pp. 4004-4016.
- Kouamé, K. F. Gioan, P., Biémi, J. et Affian, K. (1999) Méthode de cartographie des discontinuités-images satellitales: Exemple de la région semi-montagneuse à l'ouest de la Côte d'Ivoire. *Télétection*, Vol. 2, p.139-156.
- Markham, B., Storey, J., & Morfitt, R. (2015): Landsat-8 sensor characterization and calibration.

- [13]. Mhamdi, H. S., Raji, M., Maimouni, S., & Oukassou, M. (2017): Fractures network mapping using remote sensing in the Paleozoic massif of Tichka (Western High Atlas, Morocco). *Arabian Journal of Geosciences*, 10(5), 125.
- [14]. Robillard, D. (1981) : Etude stratigraphique et structurale du Moyen Atlas septentrional (région de Taza, Maroc). *Notes du Serv. Géol. Maroc*. 42 (308), 101-193.
- [15]. Segal, D. "Theoretical Basis for Differentiation of Ferric-Iron Bearing Minerals, Using Landsat MSS Data." *Proceedings of Symposium for Remote Sensing of Environment, 2nd Thematic Conference on Remote Sensing for Exploratory Geology, Fort Worth, TX (1982): 949-951.*
- [16]. Schroeder, T. A., Cohen, W. B., Song, C., Canty, M. J., & Yang, Z (2006): Radiometric correction of multi-temporal Landsat data for characterization of early successional forest patterns in western Oregon. *Remote sensing of environment*, 103(1), 16-26.
- [17]. Song et al., (2001): Classification and Change Detection Using Landsat TM Data: When and How to Correct Atmospheric Effects?
- [18]. SABINS, F.F., 1999, Remote sensing for mineral exploration, *Ore Geology Reviews*, 14, pp.157-183.
- [19]. T.D Razafinarivo et al 2017: Development of a cartographic tool for the management of pastoral resources through a combined approach of remote sensing and modeling
- [20]. United States Geological Survey: <https://www.usgs.gov/>
- [21]. Zuckerman, B., Song, I., Bessell, M. S., & Webb, R. A. (2001): The  $\beta$  Pictoris moving group. *The Astrophysical Journal Letters*, 562(1), L87.